Revealing photoluminescence and nonlinear optical absorption characteristics of $PbMo_{0.75}W_{0.25}O_4$ single crystal for optical limiting applications

Anıl Doğan[a], Ahmet Karatay[a,*], Mehmet Isık[b], Elif Akhuseyin Yildiz[a], Nizami Gasanly[c], Ayhan Elmali[a]

[a] *Department of Engineering Physics, Faculty of Engineering, Ankara University, 06100, Ankara, Turkey*

[b]*Department of Electrical and Electronics Engineering, Atilim University, 06836 Ankara, Turkey*

[c]*Department of Physics, Science and Art Faculty, Middle East Technical University, 06800 Ankara, Turkey*

ABSTRACT

Nonlinear absorption properties of $PbMo_{0.75}W_{0.25}O_4$ single crystal fabricated by the Czochralski method were studied. The band gap energy of the crystal was determined as 3.12 eV. Urbach energy which represents the defect states inside the band gap was found to be 0.106 eV. $PbMo_{0.75}W_{0.25}O_4$ single crystal has a broad photoluminescence emission band between 376 and 700 nm, with the highest emission intensity occurring at 486 nm and the lowest intensity peak at 547 nm, depending on the defect states. Femtosecond transient absorption measurements reveal that the lifetime of localized defect states is found to be higher than the 4 ns pulse duration. Open aperture (OA) Z-scan results demonstrate that the $PbMo_{0.75}W_{0.25}O_4$ crystal exhibits nonlinear absorption (NA) that includes two-photon absorption (TPA) as the dominant mechanism at the 532 nm excitations corresponding to 2.32 eV energy. NA coefficient (β_{eff}) increased from 7.24 x 10^{-10} m/W to 8.81 x 10^{-10} m/W with increasing pump intensity. At higher intensities β_{eff} tends to decrease with intensity increase. This decrease is an indication that saturable absorption (SA) occurred along with the TPA, called saturation of TPA. The lifetime of the defect states was measured by femtosecond transient absorption spectroscopy. Saturable absorption behavior was observed due to the long lifetime of the localized defect states. Closed aperture (CA) Z-scan trace shows the sign of a nonlinear refractive index. The optical limiting threshold of $PbMo_{0.75}W_{0.25}O_4$ single crystal at the lowest intensity was determined as 3.45 mJ/cm^2. Results show that the $PbMo_{0.75}W_{0.25}O_4$ single crystal can be a suitable semiconductor material for optical limiting applications in the visible region.

Keywords: $PbMo_{0.75}W_{0.25}O_4$ crystal, defect states, nonlinear absorption, optical limiting

Published by PHYSICA SCRIPTA
https://doi.org/10.1088/1402-4896/ad3aee

1. Introduction

Fabrication and testing of new materials with combinations of various organic and inorganic elements to obtain better nonlinear optical properties (multiphoton absorption, inverse saturable absorption, saturable absorption, and self-focusing/defocusing effects) is a major goal of many disciplines. Molybdate (MoO_4) and tungstate (WO_4) compounds are good host materials for metals and rare earth elements and they have a wide range of uses such as supercapacitors [1, 2], solid-state lighting [3], sensors [4], photocatalysis [5, 6], wastewater treatment [6], smart filtering optical radiation [7], microwave imaging [8], energy conversion [9], electromagnetic interference (EMI) shielding [10], optical limiting [11, 12], low temperature co-fired ceramic (LTCC) [13], and thermistor applications [14, 15]. Lead-doped crystal and thin film materials such as $PbMoO_4$ and $PbWO_4$, which are inorganic semiconductor materials, attract attention due to their high density, high chemical stability, high radiation damage threshold, high thermal conductivity, high optical transmittance, short decay time and luminescence properties in the visible region [16, 17]. It has been reported that doping metal ions such as Zn and Mn can change the optical properties of host materials by providing efficient radiation channels [18, 19]. Moreover, it has been reported that Zn-bonded WO_4 nanostructures exhibit reverse saturable absorption under continuous-wave laser excitation [20]. Besides, rare earth element doped MoO_4 and WO_4 semiconductor materials attract attention in optoelectronic technology due to their effective luminescence properties [21-24]. Additionally, these two materials are also of interest because they show nonlinear optical responses to high light intensities [11, 12, 25-29].

Within the framework of light-matter interaction, various materials in crystal [30-32], thin film [33-36], nanostructure [37], and liquid [38] forms that exhibit nonlinear absorption properties at high light intensities are produced and examined. The nonlinear effect in the transmittance of a material can be observed in two different types, nonlinear absorption (NA) and saturable absorption (SA). SA indicates the increase in transmittance depending on the increasing light intensity. This relates to the fact that at relatively low light intensities the available energy levels are filled with excited electrons and no more electrons move these levels through the valence band [39, 40]. NA corresponds to the decrease in transmittance due to increasing light intensity and is determined by the NA coefficient. The well-known NA mechanisms are one-photon absorption (OPA), two-photon absorption (TPA), free-carrier absorption (FCA), and reverse saturable absorption (RSA). The NA feature offers materials in various usage areas such as

optical switching [33], optical waveguide devices [41], ultrafast fiber lasers [42], self-defocusing lasing [43], self-frequency-doubling [44], and optical limiting [45, 46] applications.

Studies examining the optical limiting properties of materials exhibiting NA behavior are common in the literature. An optical limiter can allow light to pass up to a certain intensity threshold while absorbing light at intensities above the threshold. High-intensity light can cause serious damage to the human eye and detectors. Therefore, it is desired that the limiting threshold of an optical limiting material be as low as possible for protecting eyes and detectors. Among the nonlinear optical materials, metal MoO_4 and WO_4 materials such as Sn^{4+} doped $BaMoO_4$ [11], Cr^{3+} doped $La_2(WO_4)_3$ [12], $PbMoO_4$ [26], and Sn^{4+} doped $CdMoO_4$ [47] showed that they have good NA properties and low optical limiting thresholds.

The present work represents the investigation of the photoluminescence and nonlinear absorption properties of $PbMo_{0.75}W_{0.25}O_4$ single crystal for optical limiting applications. Structural and optical characterization of $PbMo_{0.75}W_{0.25}O_4$ single crystal was performed in our previous study [48]. For understanding the nonlinear absorption and the nonlinear refraction properties of $PbMo_{0.75}W_{0.25}O_4$ single crystal, the open aperture (OA) and closed aperture (CA) Z-scan methods were used at 532 nm laser excitations with 4 ns pulse duration and 10 Hz repetition rate. Femtosecond transition absorption spectroscopy experiments were carried out to understand the photoluminescence and nonlinear absorption mechanism of $PbMo_{0.75}W_{0.25}O_4$. The decay kinetics of $PbMo_{0.75}W_{0.25}O_4$ single crystal are discussed in detail.

Experimental Methods

A single crystal of $PbMo_{0.75}W_{0.25}O_4$ was grown using the Czochralski technique. The requisite melts, composed of PbO, MoO_3, and WO_3 oxides, were precisely combined in stoichiometric proportions within a Pt crucible for the purpose of crystal growth. This growth process involved maintaining specific rates: a pulling rate of 2 mm/h, a rotation rate of 20 rpm, and a cooling rate of 30 °C/h. Subsequently, the elongated bulk crystal obtained underwent cutting and meticulous polishing of both of its surfaces to achieve a high level of optical quality. The photograph of the crystal examined in the present paper, the x-ray diffraction pattern, and detailed information about the crystalline parameters were reported in our previous study [48]. The findings indicated that the grown compound is in single crystal form and exhibits a favorable crystalline structure. A Shimadzu-1800 model UV-VIS spectrophotometer was used to examine the linear optical absorption features of $PbMo_{0.75}W_{0.25}O_4$ single crystal. Photoluminescence measurement was performed by Pelkin Elmer LS 55 Fluorescence Spectrometer. The nonlinear optical

responses of $PbMo_{0.75}W_{0.25}O_4$ single crystal to intense laser light were investigated with the OA and CA Z-scan experiments at 532 nm wavelength excitations of Quantel Brilliant model Q-switched Nd:YAG laser source with 4 ns pulse duration, and 10 Hz repetition rate.

Ultrafast pump probe spectroscopy measurements were performed using a Ti:Sapphire laser amplifier and an optical parametric amplifier system with 52 fs pulse duration and 1 kHz repetition rate (Spectra Physics, Spitfire Pro XP, TOPAS) with a white light continuum probe a commercial pump probe experimental setup from Spectra Physics, Helios to reveal the charge transfer dynamics of $PbMo_{0.75}W_{0.25}O_4$ single crystal. Pulse duration was measured as 120 fs by cross-correlation inside the pump probe setup. The pump wavelengths were chosen based on the maximum linear absorption wavelength of the crystal. The excited state dynamics were measured between 0.1 ps and 3.2 ns timescale. Experimental data was analyzed by using Surface Xplorer software that is provided by Ultrafast Systems.

2. Results and Discussions

2.1. Linear optical properties

The linear absorption spectrum of $PbMo_{0.75}W_{0.25}O_4$ single crystal was given in Figure 1(a). there is no explicit absorption in the 500-1100 nm range. However, the absorption band corresponding to smaller wavelengths than 500 nm is close to perfect but not sharp due to the defect states localized below the conduction band. As a result, defect states are responsible for narrowing the band gap.

The band gap energy of the crystal is expressed by the Eq.1 [49], given as

$$\alpha h\nu = A\left(h\nu - E_g\right)^n \quad (1)$$

where α is the linear absorption coefficient defined from the absorption spectra, $h\nu$ is the photon energy, A is a constant, E_g is the energy of band gap, and n equals 1/2 for direct transitions and 2 for indirect transitions, respectively. The direct band gap energy of the $PbMo_{0.75}W_{0.25}O_4$ crystal was found to be 3.11 eV from the point where the linear fit line intersects the $h\nu$ axis in the Tauc plot given in Figure 1(b).

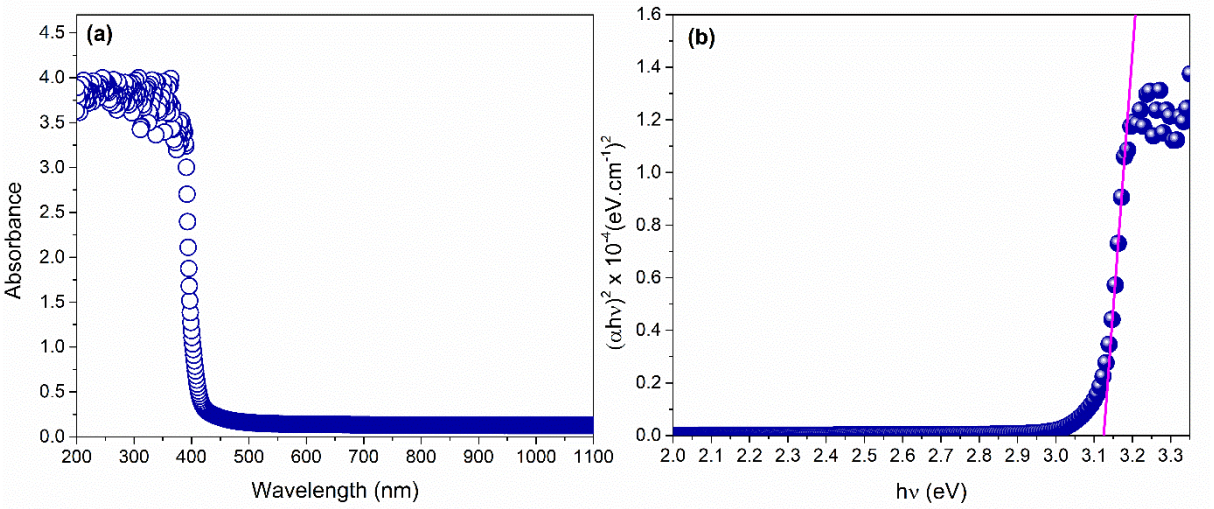

Figure 1. (a) Absorption spectrum and (b) Tauc plot of $PbMo_{0.75}W_{0.25}O_4$ single crystal.

Electronic transitions to the defect states within the band gap and close to the conduction band contribute to the NA of the $PbMo_{0.75}W_{0.25}O_4$ crystal. The Urbach energy of the crystal identifies the distribution of the defect states localized within the band gap and it can be obtained by the following equation [50],

$$\alpha = \alpha_0 \exp\left(h\nu/E_U\right) \quad (2)$$

where α_0 is a constant, and E_U is the Urbach energy. The E_U value is proportional to the defect states distributed between the valance and conduction bands. The Urbach energy of the $PbMo_{0.75}W_{0.25}O_4$ single crystal was determined as 0.106 eV from the inverse slope of the $\ln(\alpha)$ vs $h\nu$ curve illustrated in Figure 2. This result points out that the defect states are distributed below 0.106 eV of the conduction band.

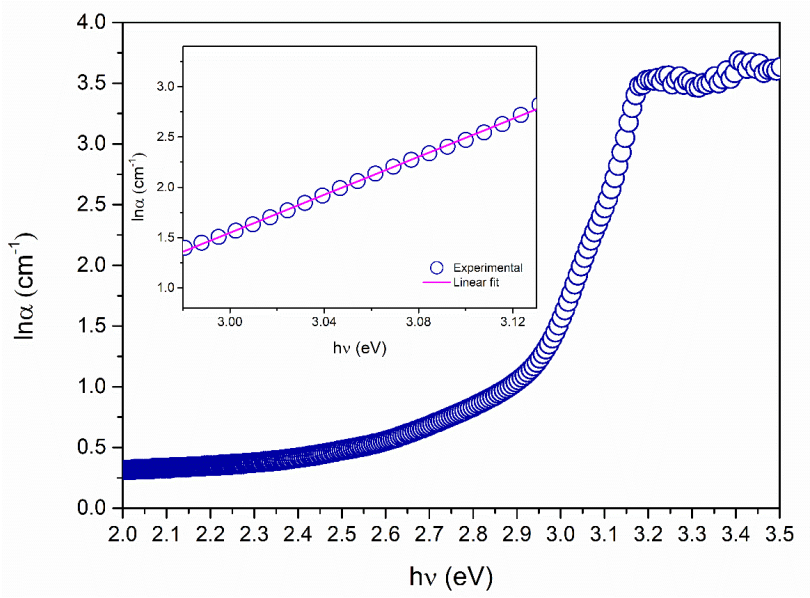

Figure 2. ln(α) vs. *hν* plot of $PbMo_{0.75}W_{0.25}O_4$ single crystal.

The photoluminescence (PL) spectrum of the $PbMo_{0.75}W_{0.25}O_4$ single crystal was obtained under 350 nm wavelength excitation and given in Figure 3. As seen in the figure, the $PbMo_{0.75}W_{0.25}O_4$ single crystal has a wide PL emission band between 376 and 700 nm. The highest emission intensity occurred at 486 nm. The lower intensity peak at 547 nm is based on the defect states. The transitions of trapped electrons from defect states localized below the conduction band to the valance band caused the emissions with lower energy. Details and a discussion of decay kinetics are given in section 2.3 Femtosecond Transient Absorption Spectroscopy. The peaks observed in the photoluminescence spectrum can be attributed to the ordered lattice defects of $[WO_4^{2-}]$ in the crystalline structure (responsible for blue emission), charge transfer transitions within $[MoO_4]$ clusters (electrons are excited from 2p states of oxygen to 4d states of Mo localized within the band gap and they emit light at different energies as they pass to different lower states during the relaxation process), and oxygen-related defect centers (responsible for green emission) [51, 52]. Photoluminescence properties can be adjusted by doping metal or rare earth elements. Shifts in the photoluminescence wavelengths were observed in molybdate and tungstate crystals doped with different alkali metals such as Ca, Cd, and Sr [53]. The emission band of the $PbMo_{0.75}W_{0.25}O_4$ single crystal is narrower than that of these crystals. It can be due to the $PbMo_{0.75}W_{0.25}O_4$ single crystal having a less defective structure than these crystals.

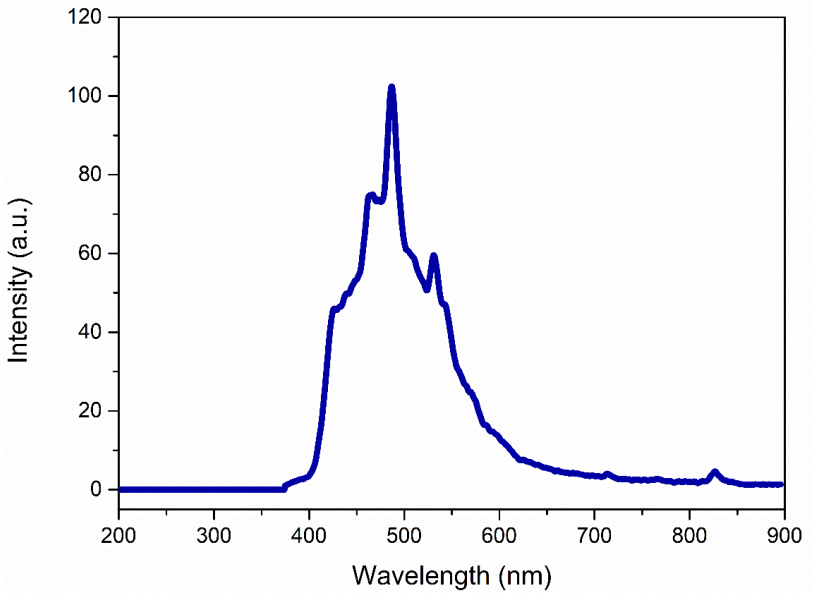

Figure 3. Fluorescence spectrum of $PbMo_{0.75}W_{0.25}O_4$ single crystal.

2.2. Nonlinear absorption properties

OA Z-scan measurements under 532 nm wavelength excitations at 4 ns pulse duration were carried out and NA behaviors of the $PbMo_{0.75}W_{0.25}O_4$ single crystal at various intensities were given in Figure 4. It can be seen in the figure that the normalized transmittance decreased with increasing input intensity. On account of the energies of defect states and excitation wavelength (532 nm) corresponding to ~3.0 eV and 2.32 eV, respectively, the electrons in the valance band do not reach defect states close to the conduction band via OPA in $PbMo_{0.75}W_{0.25}O_4$ crystal. On the other hand, the possibility of OPA occurring requires deep defect states, excitonic states, or thermally induced free carriers [54]. Since the energy of excitation light is higher than the half of band gap energy ($E_g/2$), the TPA condition is satisfied. Therefore, the dominant NA mechanism is TPA in $PbMo_{0.75}W_{0.25}O_4$ single crystal. Additionally, the defect states prohibit the recombination of electron-hole pairs and contribute to NA by trapping carriers excited by TPA. Besides, the electrons carried to the upper parts of the conduction band by TPA transfer their energies to the electrons occupying lower energy levels, and therefore, ESA contributes to NA. Another result from OA Z-scan experiments at higher input intensity excitations indicated the saturation of TPA, as seen in Figure 5. This can be explained by the fact that as higher intensities are increased, defect levels and upper excited levels begin to fill. For this reason, NA coefficients begin to decrease.

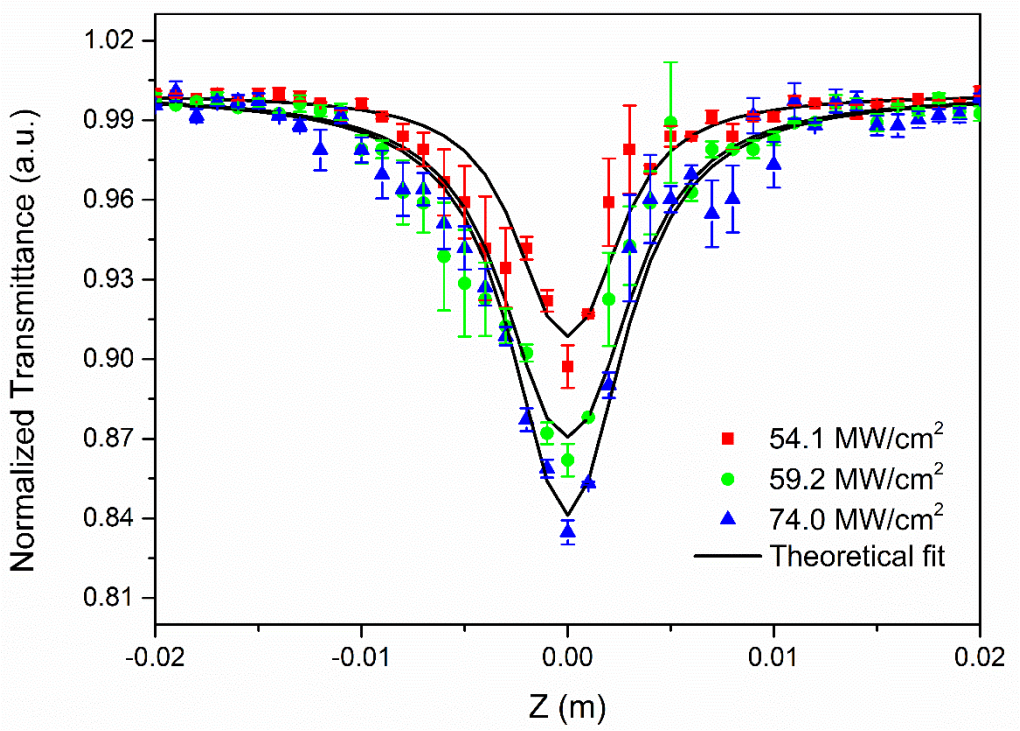

Figure 4. OA Z-scan curves of $PbMo_{0.75}W_{0.25}O_4$ single crystal with different input intensities.

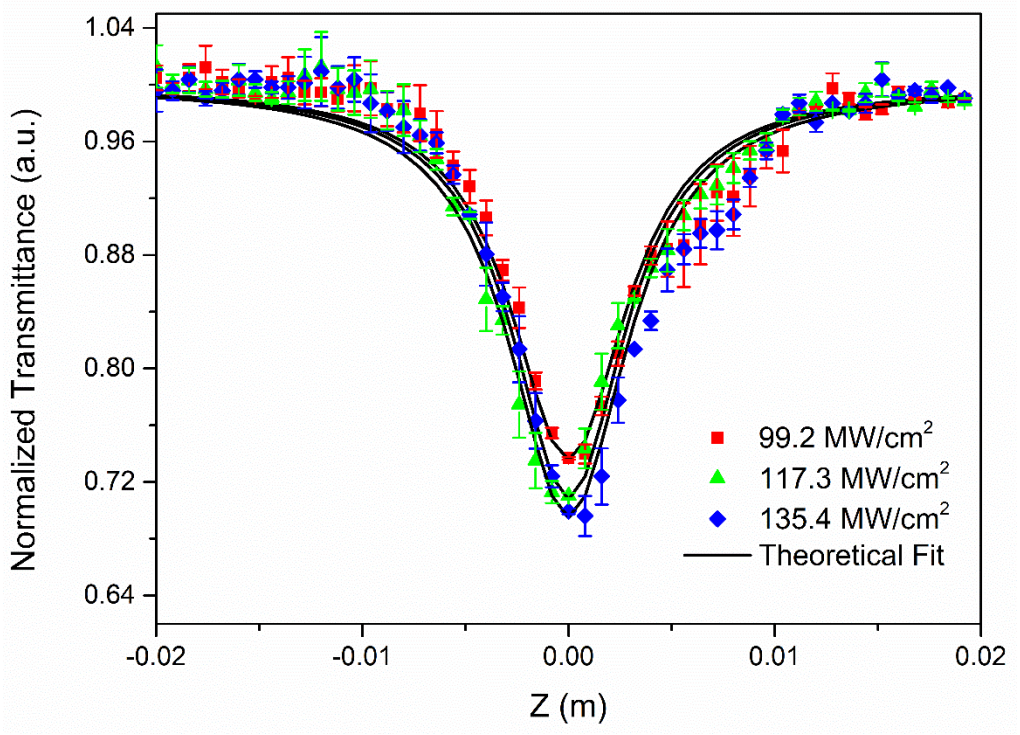

Figure 5. OA Z-scan curves of $PbMo_{0.75}W_{0.25}O_4$ single crystal at higher intensities.

A theoretical model given in Eq. (3) was used for analyzing the Z-scan results. This model represents the OPA, TPA, and free carrier absorption (FCA) and their saturations [55],

$$\frac{dI}{dz'} = -\frac{\alpha I}{1+I/I_{SAT}} - \frac{\beta I^2}{1+I^2/I_{SAT}^2} - \frac{\sigma_0 \Delta N I}{1+I^2/I_{SAT}^2} \quad (3)$$

where I is the output intensity that comes from the $PbMo_{0.75}W_{0.25}O_4$ crystal to the detector, z' is the propagation distance of light inside the crystal, I_{SAT} is the intensity threshold of saturation, β is the TPA coefficient, σ_0 is free carrier absorption cross-section. ΔN is photocarrier density and it is a function of α and β. ΔN describes the light absorption of photocarriers in defect states via OPA provided that the lifetime of the defect states is longer than the pulse duration. ΔN can be given as following equation:

$$\Delta N = \left(\sigma\tau_0/\hbar\omega_0\right) I \quad (4)$$

where τ_0 is the pulse duration and ω_0 is the beam waist at the focus. Thus, Eq. (3) becomes the following equation.

$$\frac{dI}{dz'} = -\frac{\alpha I}{1+I/I_{SAT}} - \frac{\beta_{eff} I^2}{1+I^2/I_{SAT}^2} = -f(I) \quad (5)$$

and

$$\beta_{eff} = \beta + \left(\sigma_0 \alpha \tau_0/\hbar\omega_0\right) \quad (6)$$

where β_{eff} is a free parameter obtained from the fitting of the experimental data.

The nonlinear refractive index (n_2) of the $PbMo_{0.75}W_{0.25}O_4$ crystal can be assigned from the diversity that is a function of $|\Delta\varphi_0|$ between the normalized peak (T_P) and valley transmittance (T_V) in the CA Z-scan data. The relation between the diversity and the on-axis phase shift, $|\Delta\varphi_0|$, is given as follows [56]:

$$\Delta T_{P-V} = T_P - T_V = 0.406(1-S)^{0.25}|\Delta\varphi_0| \quad (7)$$

where $S = 1 - \exp(-2r_a^2/\omega_a^2)$ is the linear aperture transmittance, r_a is the radius of the aperture and ω_a is the beam waist on the aperture. S is defined as 0.3 for this study. The nonlinear refractive index is found by the following equation.

$$n_2 = \frac{\Delta\varphi_0 \lambda}{2\pi I_0 L_{eff}} \ (cm^2/W) \quad (8)$$

where $L_{eff} = [1 - \exp(-\alpha L)]/\alpha$ is the effective thickness of the sample and I_0 is the intensity at the focus.

The pure n_2 was obtained by dividing the CA into OA data. Therefore, the CA Z-scan trace was taken into account, as shown in Figure 6. The normalized CA Z-scan trace shows prefocal transmittance valley and postfocal transmittance peak, evidence of the self-focusing ($n_2 > 0$) behavior of the $PbMo_{0.75}W_{0.25}O_4$ single crystal. The n_2 value was calculated to be 4.68 x 10^{-13} cm^2/W at 54.1 MW/cm^2 input intensity.

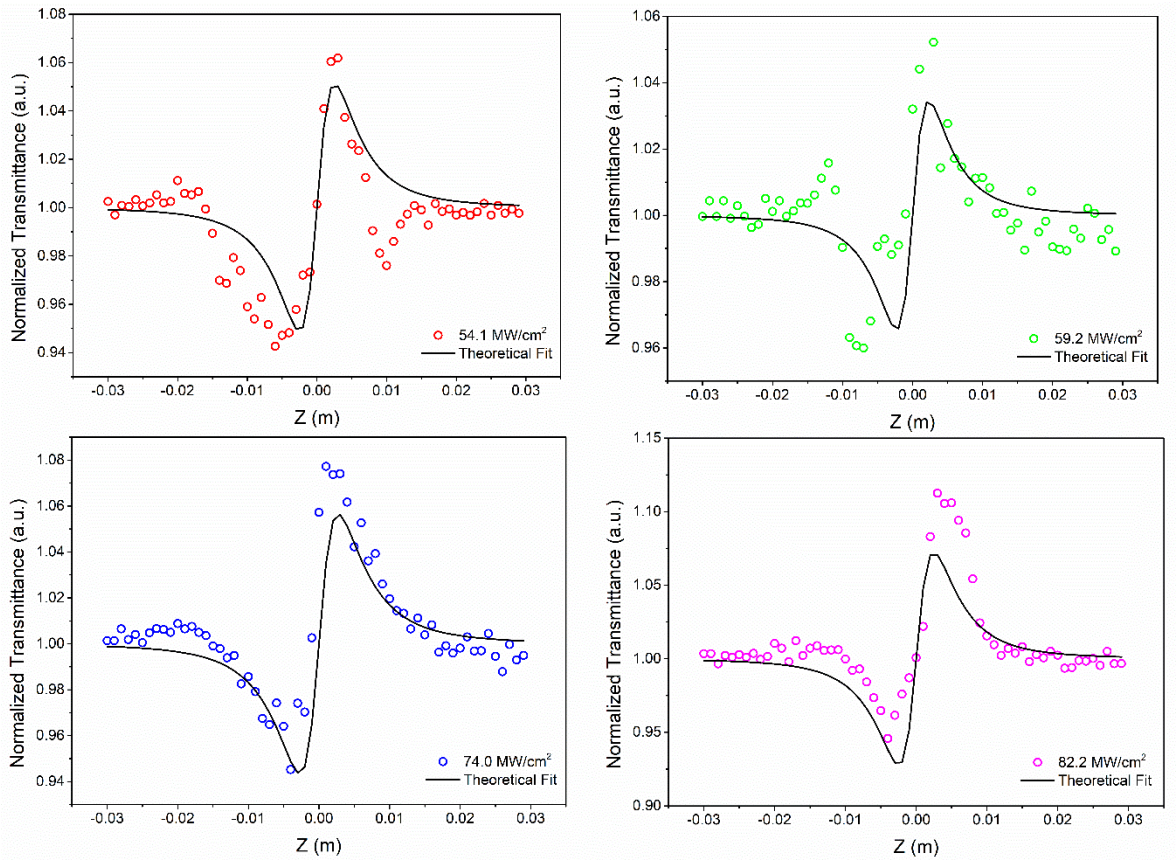

Figure 6. CA Z-scan curves of $PbMo_{0.75}W_{0.25}O_4$ single crystal at various intensities.

The obtained NA coefficients (β_{eff}) and saturation intensities (I_{SAT}) at various input intensities (I_0) from the theoretical fits of Z-scan data are listed and compared with $PbMoO_4$ and rare earth elements doped $PbWO_4$ crystals in Table 1. The β_{eff} increased from 7.24 x 10^{-10} m/W to 8.81 x 10^{-10} m/W with increasing pump intensity. At higher intensities, the β_{eff} values tended to decrease from 1.51 x 10^{-9} m/W to 1.36 x 10^{-9} m/W with increasing input intensity. I_{SAT} is the input intensity value required for saturable absorption (SA) to occur. Unlike $PbMoO_4$ and $PbWO_4$ crystals, the decrease in the β_{eff} values of $PbMo_{0.75}W_{0.25}O_4$ crystal with increasing input intensity is a consequence of the fact that SA also occurred along with TPA, called saturation of TPA. The $PbMo_{0.75}W_{0.25}O_4$ single crystal we studied has lower nonlinear

absorption coefficients than that of the other crystals as referenced in Table 1. The reason for this is the less defective structure of the $PbMo_{0.75}W_{0.25}O_4$ single crystal than the others, and then the nonlinear effect occurs at relatively higher laser intensities and initiates saturation. At low intensities, the $PbMo_{0.75}W_{0.25}O_4$ crystal did not show nonlinear properties. The nonlinear effects were observed in molybdate and tungstate crystals at relatively lower laser intensities as seen in Table 1. Accordingly, it is seen that the alkaline metal contribution, Mo and W ratios, and their combinations affect the nonlinear absorption and optical limiting properties, and these effects can be adjusted. However, since the band gap energies of these crystals are in 3-5 eV range, optical limiting cannot be achieved for the near-infrared region.

Table 1. Comparison of I_{SAT} and β_{eff} values of $PbMo_{0.75}W_{0.25}O_4$ crystal with different studies on $PbMoO_4$ and $PbWO_4$ crystals with excitation wavelengths and pulse durations (τ).

Materials	λ_{exc}(nm)	τ (ns)	I_0 (MW/cm^2)	I_{SAT} (W/m^2)	β_{eff} (m/W)	Refs
$PbMo_{0.75}W_{0.25}O_4$	532	4	54.1	1.40×10^{12}	7.24×10^{-10}	present work
single crystal			59.2	7.45×10^{12}	8.50×10^{-10}	
			74.0	4.15×10^{12}	8.81×10^{-10}	
			99.2	1.08×10^{12}	1.51×10^{-9}	
			117.3	1.40×10^{12}	1.38×10^{-9}	
			135.4	1.29×10^{11}	1.36×10^{-9}	
$PbMoO_4$	532	4	2.16	3.20×10^{11}	7.11×10^{-8}	[26]
single crystal			853	3.51×10^{11}	8.26×10^{-8}	
			13.05	3.79×10^{11}	9.46×10^{-8}	
			19.42	3.84×10^{11}	1.96×10^{-7}	
$PbWO_4$: (0%) Mn^{2+}	532	10	-	0.5106×10^{9}	1.496×10^{-10}	[27]
$PbWO_4$: (0.3%) Mn^{2+}				0.9855×10^{9}	1.980×10^{-10}	
$PbWO_4$: (0.5%) Mn^{2+}				1.4027×10^{9}	2.029×10^{-10}	
$PbWO_4$: (0.7%) Mn^{2+}				2.3392×10^{9}	2.496×10^{-10}	
$PbWO_4$: (0%) Cr^{3+}	532	-	-	-	1.32×10^{-6}	[28]
$PbWO_4$: (0.1%) Cr^{3+}					1.52×10^{-6}	
$PbWO_4$: (0.3%) Cr^{3+}					1.78×10^{-6}	
$PbWO_4$: (0.5%) Cr^{3+}					1.83×10^{-6}	
$PbWO_4$: (0.7%) Cr^{3+}					2.31×10^{-6}	
$ZnMoO_4$	532	-	-	-	2.15×10^{-6}	[29]
$ZnMoO_4$: Ni (0.3%)					2.84×10^{-6}	
$ZnMoO_4$: Ni (0.5%)					2.52×10^{-6}	
$ZnMoO_4$: Ni (0.7%)					2.19×10^{-6}	

$ZnMoO_4$: Ni (0.9%)					3.31×10^{-6}	
$ZnWO_4$	532	-	-	-	3.36×10^{-8}	
$ZnWO_4$: Er (0.3%)					3.92×10^{-8}	
$ZnWO_4$: Er (0.5%)					4.27×10^{-8}	[20]
$ZnWO_4$: Er (0.7%)					4.82×10^{-8}	
$ZnWO_4$: Er (0.9%)					5.13×10^{-8}	
$(CoMoO4)_4$/PMMA	532	6	33	-	1.75×10^{-5}	
microcrystal			48		1.23×10^{-5}	
			63		1.01×10^{-5}	[57]
			82		0.80×10^{-5}	
			86		0.68×10^{-5}	

The optical limiting threshold of $PbMo_{0.75}W_{0.25}O_4$ single crystal was defined from the normalized transmission curve as a function of fluence, as seen in Figure 7. The decrease in the normalized transmittance with increasing fluence of light gives the $PbMo_{0.75}W_{0.25}O_4$ single crystal an optical limiting feature that can be identified with a limiting threshold refers to the point of fluence where the transmittance starts to strongly fall. The optical limiting threshold of $PbMo_{0.75}W_{0.25}O_4$ single crystal was found as 3.45 mJ/cm^2 at 54.1 MW/cm^2 input intensity. In the previous study, the optical limiting threshold was found as 4.91 mJ/cm^2 at 2.16 MW/cm^2 for $PbMoO_4$ single crystal [26]. This result shows that the $PbMo_{0.75}W_{0.25}O_4$ crystal exhibits better optical limiting performance at greater input intensities compared to the previous study. Besides, the optical limiting threshold of $PbMo_{0.75}W_{0.25}O_4$ was compared with MoO_4 and WO_4 based materials with various components in the literature and listed in Table 2.

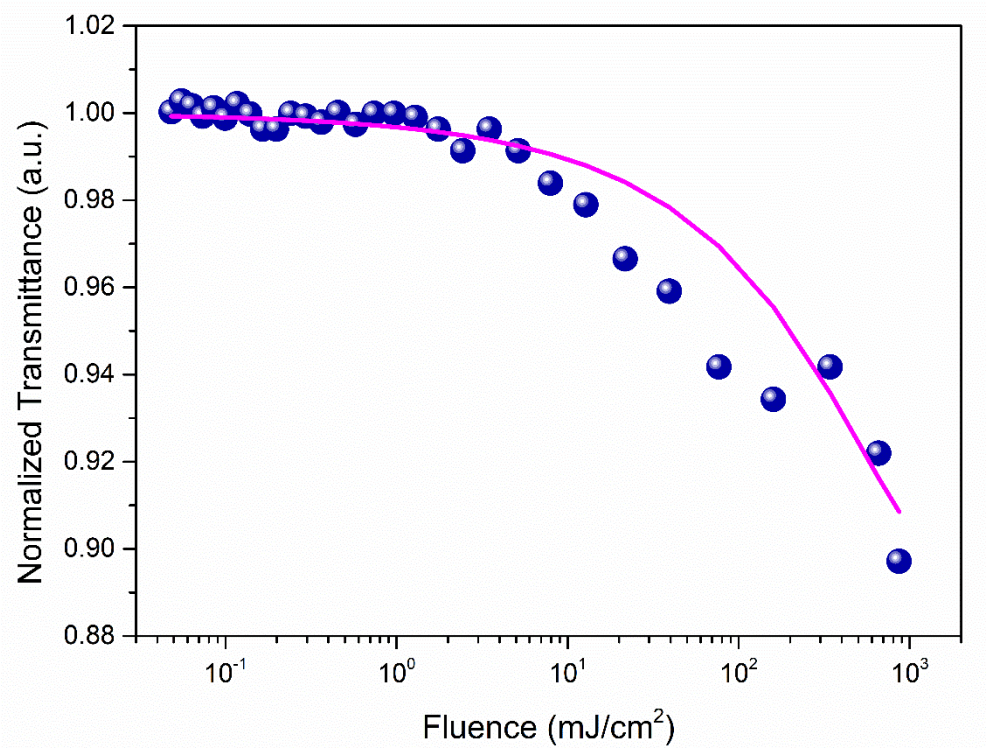

Figure 7. Optical limiting curve of $PbMo_{0.75}W_{0.25}O_4$ single crystal at 54.1 MW/cm^2 input intensity.

Table 2. Comparison of the optical limiting thresholds of $PbMo_{0.75}W_{0.25}O_4$ single crystal and MoO_4 and WO_4 based materials in the literature.

Materials	Optical limiting thresholds	References
$PbMo_{0.75}W_{0.25}O_4$	3.45 mJ/cm^2	Present work
$BaMoO_4$	221 MW/cm^2	[11]
$Sn_{0.1}Ba_{0.9}MoO_4$	136 MW/cm^2	
$Sn_{0.3}Ba_{0.7}MoO_4$	109 MW/cm^2	
$Sn_{0.5}Ba_{0.5}MoO_4$	204 MW/cm^2	
$La_2(WO_4)_3$	91.2 W/cm^2	[12]
$La_2(WO_4)_3$: Cr^{3+} (0.1%)	87.1 W/cm^2	
$La_2(WO_4)_3$: Cr^{3+} (0.3%)	86.9 W/cm^2	
$La_2(WO_4)_3$: Cr^{3+} (0.5%)	86.7 W/cm^2	
$La_2(WO_4)_3$: Cr^{3+} (0.7%)	86.2 W/cm^2	
$PbMoO_4$	4.91 mJ/cm^2	[26]
$CdMoO_4$	41.45 J/cm^2	[47]
$Sn_{0.1}Cd_{0.9}MoO_4$	32.83 J/cm^2	
$Sn_{0.3}Cd_{0.9}MoO_4$	21.22 J/cm^2	

$Sn_{0.5}Cd_{0.9}MoO_4$	11.92 J/cm^2	
$(CoMoO4)_4$/PMMA	1.99 J/cm^2	
$(CoMoO4)_6$/PMMA	1.48 J/cm^2	[57]
$(CoMoO4)_8$/PMMA	1.31 J/cm^2	

2.3 Femtosecond Transient Absorption Spectroscopy

In an attempt to understand photoluminescence and nonlinear absorption mechanism and decay kinetics of $PbMo_{0.75}W_{0.25}O_4$ crystal femtosecond transient absorption spectroscopy measurements were carried out. The pump wavelength was determined as 400 nm corresponding to the edge of the energy band gap of the crystal. Thus, the defect states localized under the conduction band were also excited. In transient absorption spectra of $PbMo_{0.75}W_{0.25}O_4$ crystal, it was observed that there is a broad and continuous excited state absorption (ESA) band in the range of 400-800 nm as expected nature of the semiconductors (Figure 8). The strong ESA signal around 450 nm can be originated from the localized defect state. It was also observed that the maxima of the ESA signal red shifted with time delay due to filling of the defect states. Possible transitions between the energy states are shown in Figure 9.

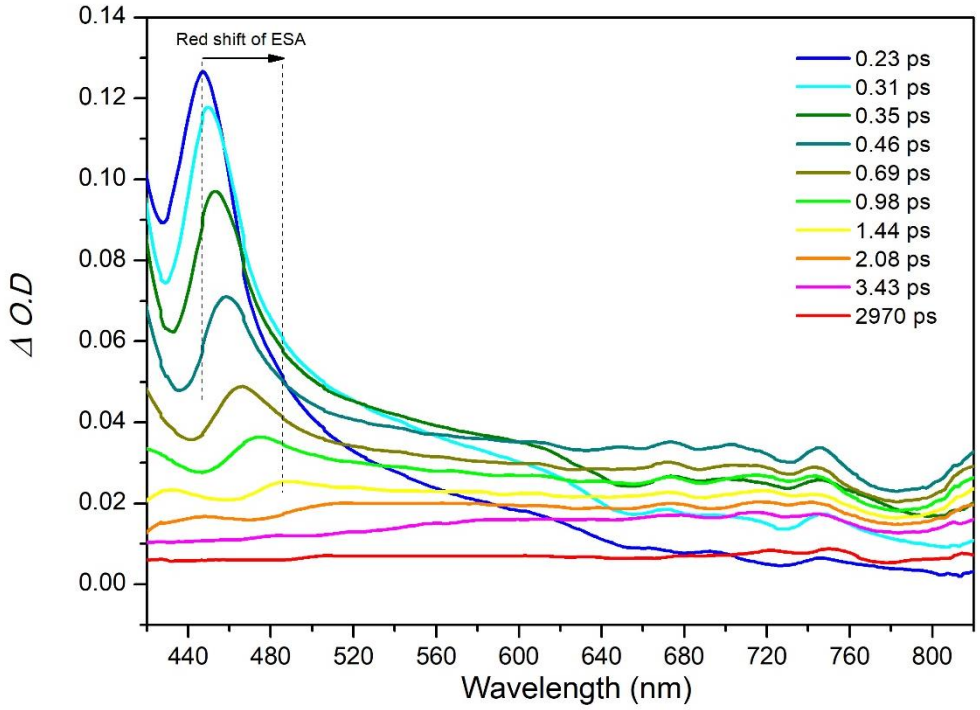

Figure 8. Transient absorption spectra of $PbMo_{0.75}W_{0.25}O_4$ crystal with 400 nm excitation.

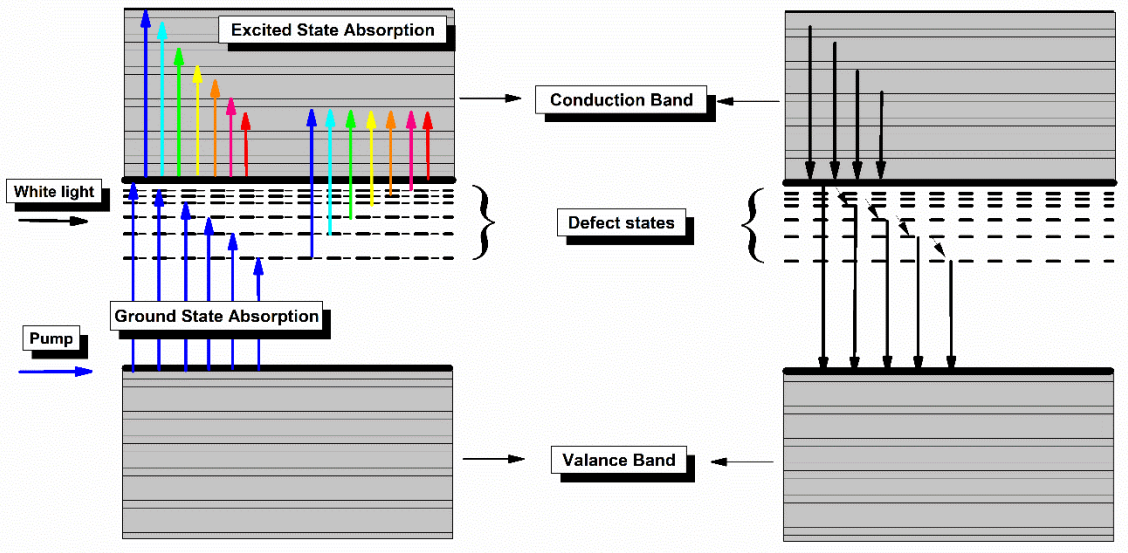

Figure 9. Possible optical transitions of $PbMo_{0.75}W_{0.25}O_4$ crystal with 400 nm excitation.

Saturable absorption property occurs only if the lifetime of the localized defect states is longer than the pulse duration of the laser. To get deep insight into the dynamics of the defect states, the decay kinetics were fitted using Surface Xplorer software with the function as given [58],

$$I(t) = \int R(t - t')S(t')dt' \quad (9)$$

where $I(t)$ is the time-resolved intensity, $R(t)$ is the instrument response function and $S(t)$ is the response from the crystal, respectively.

The salient features of nonlinear dynamics in semiconductors under optical excitation have been studied in the literature [59-61]. The understanding of the transient processes occurring in photo-generated carrier populations is of great relevance because it would allow a deeper physical insight on the dynamical effects of interaction mechanisms upon observable properties of the system. The first of them, commonly called the thermalization process, is mainly governed by the rapid interactions, namely, the electron-electron and the electron-optical phonon interactions. In this stage the carrier distribution function is far from equilibrium. Once thermalized, the electronic system relaxes by dissipating the energy in excess into the lattice. This stage ends when the interaction mechanisms randomize the energy and momentum in the carrier population. The second stage of the relaxation is the so called, cooling process, and is mainly ruled by the slow interactions in the system, namely, electron-phonon scattering and recombination. Associated to each one of the stages of the relaxation process, there is a characteristic time. The first one, the thermalization time, is an effective time determined by the intrinsic characteristic times of the rapid interaction mechanisms within the system and the

second one is a characteristic time determined by the interaction mechanisms of the system with the surroundings. Carrier thermalization is a relatively fast process, typically in the range of 10 fs to 1 ps. Semiconductors typically have some shallow or deep sub-bandgap defect states. Carriers from the band-edge quickly get trapped into these states within a short span of 10–100 ps. More the number of traps faster is the trapping rate [62]. Further decay of excess carriers take place through band-to-band or excitonic radiative recombination. The radiative recombination lifetime of typical compound semiconductors is in the range of 0.1–100 ns [62].

The decay traces of $PbMo_{0.75}W_{0.25}O_4$ crystal by probing 450 nm and 600 nm are given in Figure 10. The transient absorption signal caused by the excited carrier absorption in the $PbMo_{0.75}W_{0.25}O_4$ crystal immediately appears after the pump excitation. The fast component around 100 fs indicates that the photo-excited carriers complete the thermalization through carrier-carrier scattering in $PbMo_{0.75}W_{0.25}O_4$ crystal. The second component in the order of a few picoseconds can be attributed to the charge recombination with getting trapped by the localized defect states. The time components are about 9 ps and 11 ps for 450 nm and 600 nm probe wavelengths, respectively. Finally, the slow component (out of the time scale range in pump-probe setup) is attributed to the carrier vanishing from localized defect states to valence band for electron-hole recombination. This time scale is compatible with the radiative recombination lifetime of typical compound semiconductors, as the results also prove that PL signals originate from defect states [62]. Since the trapping lifetime of the crystal is higher than the laser pulse duration (4 ns), the SA properties were observed under high intensities.

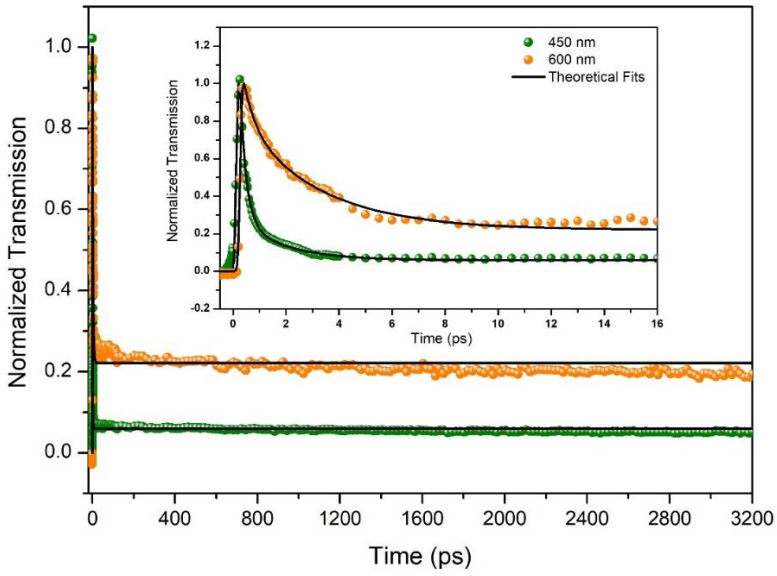

Figure 10. Decay traces of the nonlinear absorption at 400 nm excitation of $PbMo_{0.75}W_{0.25}O_4$ crystal.

4. Conclusion

$PbMo_{0.75}W_{0.25}O_4$ single crystal fabricated by the Czochralski technique and nonlinear absorption properties were investigated. The band gap and Urbach energies of $PbMo_{0.75}W_{0.25}O_4$ crystal were calculated as 3.12 and 0.106 eV. $PbMo_{0.75}W_{0.25}O_4$ single crystal has a broad PL emission band from 376 to 700 nm depending on defect states. Results of the OA Z-scan experiment at 532 nm excitations with 4 ns pulse duration indicate that the $PbMo_{0.75}W_{0.25}O_4$ crystal has NA and SA behavior. Based on the femtosecond transient absorption measurements, the lifetime of the localized defect states was found higher than 4 ns pulse duration. This explains why open aperture Z-scan experiments exhibit saturable absorption characteristics with high intensities. TPA is the dominant mechanism of NA at 532 nm excitations corresponding to 2.32 eV. Since the defect states close to the conduction band, OPA does not contribute to NA. β_{eff} increased from 7.24 x 10^{-10} m/W to 8.81 x 10^{-10} m/W with increasing pump intensity. At higher intensities, β_{eff} indicated a decreasing trend due to the saturation of TPA. The higher nonlinear refractive index was found to be 4.68 x 10^{-13} cm^2/W at 54.1 MW/cm^2 input intensity. The optical limiting threshold of $PbMo_{0.75}W_{0.25}O_4$ single crystal was found as 3.45 mJ/cm^2. As a result, $PbMo_{0.75}W_{0.25}O_4$ single crystal can be a promising optical limiter material in the visible region.

REFERENCES

[1] Yua D Y, Meng Y N, Liu L Y, Wu Y P, Liu X Y 2022 Rapid microwave-assisted synthesis strategy of dual-cationic molybdates as high-performance electrodes for alkaline battery-supercapacitor hybrid devices J Alloy Compd **920**.

[2] Sorouri A M, Sobhani-Nasab A, Ganjali M R, Manani S, Ehrlich H, Joseph Y, Rahimi-Nasrabadi M 2023 Metal tungstates nanostructures for supercapacitors: A review Appl Mater Today **32**.

[3] Han Z, Wang X Y, Fu B, Yan H K, Liao J S 2022 Novel double molybdate LiLu(MoO4)(2):Sm3+ red phosphors with excellent thermal stability for white LEDs J Lumin **252**.

[4] Lin Z D, Xu M Y, Fu P, Deng Q R 2018 Crystal plane control of 3D iron molybdate and the facet effect on gas sensing performances Sensor Actuat B-Chem **254** 755-62.

[5] Karthik R, Karikalan N, Chen S M, Kumar J V, Karuppiah C, Muthuraj V 2017 Assessment of divergent functional properties of seed-like strontium molybdate for the photocatalysis and electrocatalysis of the postharvest scald inhibitor diphenylamine J Catal **352** 606-16.

[6] Abubakar H L, Tijani J O, Abdulkareem S A, Mann A, Mustapha S 2022 A review on the applications of zinc tungstate (ZnWO4) photocatalyst for wastewater treatment Heliyon **8**.

[7] Madhubala V, Sahni A, Sujatha R A 2023 Optical nonlinear effects of nickel and cobalt substituents in 1D/2D manganese tungstate/rGO nanocomposite for smart filtering optical radiation J Photoch Photobio A **438**.

[8] Li F Y, Li Y X, Luo Y, Zhang J P, Lu Y C, Peng R, Tang T T, Wen Q Y 2023 Enhanced Cu2+-substituted zinc molybdate low temperature co-fired ceramics for static microwave imaging applications J Alloy Compd **945**.

[9] Swathi S, Yuvakkumar R, Kumar P S, Ravi G, Thambidurai M, Dang C, Velauthapillai D 2022 PEG mediated tetragonal calcium molybdate nanostructures for electrochemical energy conversion applications Int J Hydrogen Energ **47** 26013-22.

[10] Taj M N, Prasad B D, Narapareddy R, Nagabhushana H, Ramakrishna G, Mahesh B, Dadami S T 2022 PANI-molybdate nanocomposites: Structural, morphological and dielectric properties for the effective electromagnetic interference (EMI) shielding applications in X-band Appl Surf Sci Adv **7**.

[11] Binish B, Durairaj M, Girisun T C S, Rahulan K M 2023 Engineering the nonlinear optical properties of barium molybdate by doping Sn4+ ions for optical limiting device applications Ceram Int **49** 17629-38.

[12] Karthikeyan D, Vijayakumar K, Suhasini P, Dhanusha A, Girisun T C S 2023 Third-order nonlinear optical responses of Cr3+ions on La2(WO4)3 nanoparticles for optical limiting applications J Photoch Photobio A **436**.

[13] Wei X L, He Y H, Tang M L, Yang J H, Wu Y, Chen X L, Zhou H F 2023 Microwave dielectric properties of ternary molybdate NaSrLn(MoO4)(3) (Ln = Nd, Sm) ceramics for LTCC applications Ceram Int **49** 23864-70.

[14] Panda D, Hota S S, Choudhary R N P 2023 Development of a novel triple perovskite barium bismuth molybdate material for thermistor-based applications Mater Sci Eng B-Adv **296**.

[15] Hota S S, Panda D, Choudhary R N P 2023 Studies of structural, dielectric, and electrical properties of polycrystalline barium bismuth tungstate for thermistor application Inorg Chem Commun **153**.

[16] Arularasu M V, Sundaram R, Magdalane C M, Kanimozhi K, Kaviyarasu K, Thema F T, Letsholathebe D, Mola G T, Maaza M 2017 Synthesis, Humidity Sensing, Photocatalytic and Antimicrobial Properties of Thin Film Nanoporous PbWO-WO Nanocomposites J Nanostruct **7** 47-56.

[17] Vernaleken A, Cohen M G, Metcalf H 2007 Interferometric measurement of acoustic velocity in PbMoO and TeO Applied Optics **46** 7117-9.

[18] Xie A, Yuan X M, Wang F X, Shi Y, Mu Z F 2010 Enhanced red emission in ZnMoO:Eu by charge compensation J Phys D Appl Phys **43**.

[19] Anugop B, Prasanth S, Raj D R, Vineeshkumar T V, Pranitha S, Pillai V P M, Sudarsanakumar C 2016 Role of Mn concentration in the linear and nonlinear optical properties of NiMnSe nanoparticles Opt Mater **62** 297-305.

[20] Rahulan K M, Flower A L, Padmanathan N, Mahendra A, Shekhawat V, Vinitha G, Sujatha R A, Shivkumar M A 2020 Luminescence and nonlinear optical properties of Er3+ - doped ZnWO4 nanostructures J Photoch Photobio A **386**.

[21] Dutta S, Som S, Priya J, Sharma S K 2013 Band gap, CIE and trap depth parameters of rare earth molybdate phosphors for optoelectronic applications Solid State Sci **18** 114-22.

[22] Nagpal D, Bhadauria T, Jayasimhadri M 2022 Structural and spectroscopic studies of Eu3+activated potassium bismuth molybdate phosphor for optoelectronic device applications Mater Today-Proc **62** 3719-23.

[23] Sarkar J, Mondal S, Panja S, Dey I, Sarkar A, Ghorai U K 2019 Multicolour tuning and perfect white emission from novel PbWO4:Yb3+ :Ho3+ :Tm3+ nanophosphor Mater Res Bull **112** 314-22.

[24] Pradeep S G, Sreedharan R S, Suresh S, Kavitha V S, Pillai N V, Pillai V P M 2020 Luminescent Tb3+ doped barium tungstate thin films as a potential candidate for photonic applications J Lumin **226**.

[25] Bhabu K A, Balaji S R, Devi R S, Balu T, Muralidharan G, Rajasekaran T R 2016 Investigations on growth and characterization of glycine admixture sodium molybdate crystals for nonlinear optical applications Optik **127** 1708-13.

[26] Pepe Y, Isik M, Karatay A, Gasanly N, Elmali A 2022 Nonlinear optical absorption characteristics of PbMoO4 single crystal for optical limiter applications Opt Mater **133**.

[27] Divya P, Flower N A L, Sujatha R A, Padmanathan N, Rose P, Saif S, Rahulan K M 2022 Structural and nonlinear optical absorption studies of Mn doped PbWO4 nanoparticles J Photoch Photobio A **426**.

[28] Divya P, Sujatha R A, Flower N A L, Vinitha G, Rahulan K M 2022 Third order nonlinear optical absorption studies of Cr3+ doped PbWO4 nanostructures Opt Mater **134**.

[29] Jayasree A S, Rahulan K M, Sujatha R A, Vinitha G, Flower N A L 2022 Influence of Ni doping on the structural and third order nonlinear optical properties of ZnMoO4 nanostructures Ceram Int **48** 29267-73.

[30] Muthuraja A, Bharath D, Murugesan G, Anbuselvi D, Kalainathan S 2022 Nonlinear optical studies on bioperine crystals grown by vertical Bridgman technique for photonic applications Opt Laser Technol **149**.

[31] Karatay A 2019 Controlling of two photon absorption properties by altering composition ratio of GaSSe crystals Opt Laser Technol **111** 6-10.

[32] Karatay A, Yuksek M, Ertap H, Mak A K, Karabulut M, Elmali A 2016 Influence of boron concentration on nonlinear absorption and ultrafast dynamics in GaSe crystals Opt Mater **60** 74-80.

[33] Lee K, Lee I H, Khim Y G, Kwon S Y, Lim G, Jung J, Chang Y J, Lee J H 2023 Nonlinear optical properties of PVD-grown Cr2Te3 film and its nonlinear switching application J Alloy Compd **956**.

[34] Ünlü B A, Sener D, Tekin S, Yildiz E A, Karatay A, Serin T, Elmali A 2021 Enhancement of Nonlinear Absorption in Defect Controlled ZnO Polycrystalline Thin Films by Means of Co-Doping Phys Status Solidi B **258**.
[35] Ünlü B A, Karatay A, Yüksek M, Ünver H, Gasanly N, Elmali A 2020 The effect of Ga/In ratio and annealing temperature on the nonlinear absorption behaviors in amorphous TlGaInS ($0 \leq x \leq 1$) chalcogenide thin films Opt Laser Technol **128**.

[36] Karatay A, Küçüköz B, Çankaya G, Ates A, Elmali A 2017 The effect of Se/Te ratio on transient absorption behavior and nonlinear absorption properties of CuInGa(SeTe) ($0 \leq x \leq 1$) amorphous semiconductor thin films Opt Mater **73** 20-4.

[37] Shanthi S, Flower N A L, Sujatha R A, Vinitha G, Rahulan K M 2023 Role of defects on the nonlinear optical properties of La doped Bi2WO6 nanostructures for optical device applications Opt Mater **136**.
[38] Al-Hamdani U J, Hassan Q M A, Zaidan A M, Sultan H A, Hussain K A, Emshary C A, Alabdullah Z T Y 2022 Optical nonlinear properties and all optical switching in a synthesized liquid crystal J Mol Liq **361**.
[39] Xiao X C, Zhu H X, Wang C, Wang Y W, Chen Z H, Xiao S, Zhong M Z, He J 2022 Saturable absorption and reverse saturable absorption of CdGa2Se4 nanoparticles determined by bond strength Phys Lett A **449**.
[40] Pepe Y, Isik M, Karatay A, Yildiz E A, Gasanly N, Elmali A 2022 The role of defects on the transition from saturable absorption to nonlinear absorption of Bi12GeO20 single crystal under increasing laser excitation J Lumin **251**.
[41] Cao X M, Peng J, Wang W Q, Xu W Q, Xu S P 2023 An elastic luminescent organic single crystal with linear and nonlinear optical waveguide properties Dyes Pigments **219**.
[42] Guo J, Liu Z H, Wageh S, Al-Hartomy O A, Al-Sehemi A G, Ge Y Q, He W L, Wei S R, Bao W L, Zhang H 2023 Ta2C MXene: Nonlinear optical properties and application in femtosecond fiber laser Opt Laser Technol **161**.
[43] Nayak D, Vijayan N, Kumari M, Kiran, Vashishtha P, Das S, Sridhar B, Gupta G, Pant R P 2022 Investigation on synthesis, growth, Hirshfeld surface and third order nonlinear optical properties of Urea-Succinic Acid single crystal: A potential candidate for self-defocusing lasing application Opt Mater **124**.
[44] Chen F F, Wang L J, Wang X L, Cheng X F, Yu F P, Wang Z P, Zhao X 2017 Single crystal growth and nonlinear optical properties of Nd3+ doped STGS crystal for self-frequency-doubling application Opt Mater **73** 33-7.
[45] Saravanan M, Girisun T C S 2017 Enhanced nonlinear optical absorption and optical limiting properties of superparamagnetic spinel zinc ferrite decorated reduced graphene oxide nanostructures Appl Surf Sci **392** 904-11.
[46] Ünlü B A, Karatay A, Yildiz E A, Dinçbay T, Ünver H, Gasanly N, Elmali A 2022 Defect assisted nonlinear absorption and optical limiting in amorphous TlGaSSe ($0 \leq x \leq 1$) thin films J Lumin **241**.

[47] Binish B, Rahulan K M 2023 Synergic effects of Sn4+doping on the nonlinear optical limiting properties of SnxCd1-xMoO4 nanostructures for optoelectronic applications J Photoch Photobio A **439**.
[48] Isik M, Gasanly N M, Darvishov N H, Bagiev V E 2023 Growth and characterization of PbMo0.75W0.25O4 single crystal: A promising material for optical applications Mater Chem Phys **296**.
[49] Tauc J 1968 Optical properties and electronic structure of amorphous Ge and Si Mater Res Bull **3** 37–46.

[50] Urbach F 1953 The Long-Wavelength Edge of Photographic Sensitivity and of the Electronic Absorption of Solids Phys Rev **92** 1324-.
[51] Pang H F, Gu M L, Li B H, Zhang T 2018 Effect of sintering temperature on the structural and luminescence properties of Er doped PbWO microcrystals Appl Phys a-Mater **124**.

[52] Sczancoski J C, Cavalcante L S, Marana N L, da Silva R O, Tranquilin R L, Joya M R, Pizani P S, Varela J A, Sambrano J R, Li M S, Longo E, Andrés J 2010 Electronic structure and optical properties of BaMoO powders Curr Appl Phys **10** 614-24.

[53] Ahmed N, Krau H, Kim H J, Mokina V, Tsiumra V, Wagner A, Zhydachevskyy Y, Mykhaylyk V B 2018 Characterisation of tungstate and molybdate crystals ABO4 (A = Ca, Sr, Zn, Cd; B = W, Mo) for luminescence lifetime cryothermometry Materialia **4** 287-96.
[54] Unlu B A, Bilir G, Yuksek M, Karatay A, Yildiz E A, Elmali A 2022 Mechanisms of nonlinear optical absorption in (GeO2)(1-x)-(PbF2)(x) (0.1 <= x <= 0.3) modified germanate glasses Opt Mater **131**.
[55] Yuksek M, Kurum U, Yaglioglu H G, Elmali A, Ates A 2010 Nonlinear and saturable absorption characteristics of amorphous InSe thin films Journal of Applied Physics **107**.
[56] Sheikbahae M, Said A A, Wei T H, Hagan D J, Vanstryland E W 1990 Sensitive Measurement of Optical Nonlinearities Using a Single Beam Ieee J Quantum Elect **26** 760-9.
[57] Wang P Y, Wang Y T, Yuan C G, Chen B K, Zhang T J, Li B C, Ouyang Q Y 2022 Nonlinear absorption, refraction and optical limiting properties of cobalt molybdate microcrystals Opt Mater **124**.
[58] Dong P T, Cheng J X 2017 Pump-Probe Microscopy: Theory, Instrumentation, and Applications Spectroscopy-Us **32** 24-36.
[59] Othonos A 1998 Probing ultrafast carrier and phonon dynamics in semiconductors Journal of Applied Physics **83** 1789-830.
[60] Cabanillas-Gonzalez J, Grancini G, Lanzani G 2011 Pump-Probe Spectroscopy in Organic Semiconductors: Monitoring Fundamental Processes of Relevance in Optoelectronics Adv Mater **23** 5468-85.
[61] Piprek J, Römer F, Witzigmann B 2015 On the uncertainty of the Auger recombination coefficient extracted from InGaN/GaN light-emitting diode efficiency droop measurements Appl Phys Lett **106**.
[62] Aggarwal T, Udai A, Banerjee D, Pendem V, Chouksey S, Saha P, Sankaranarayanan S, Ganguly S, Bhattacharya P, Saha D 2021 Investigation of Ultrafast Carrier Dynamics in InGaN/GaN-Based Nanostructures Using Femtosecond Pump-Probe Absorption Spectroscopy Phys Status Solidi B **258**.